We are IntechOpen, the world's leading publisher of Open Access books Built by scientists, for scientists

5,300
Open access books available

130,000
International authors and editors

155M
Downloads

154
Countries delivered to

Our authors are among the

TOP 1%
most cited scientists

12.2%
Contributors from top 500 universities

CLARIVATE ANALYTICS
BOOK CITATION INDEX
INDEXED

WEB OF SCIENCE™

Selection of our books indexed in the Book Citation Index
in Web of Science™ Core Collection (BKCI)

Interested in publishing with us?
Contact book.department@intechopen.com

Photocatalytic Properties of Commercially Available TiO₂ Powders for Pollution Control

Manuel Nuño, Richard J. Ball and Chris R. Bowen

Additional information is available at the end of the chapter

Abstract

The photocatalytic properties of titanium dioxide have been widely studied over recent decades since the discovery of water photolysis by TiO₂ electrodes in 1972. Titanium dioxide has three main crystal polymorphs; anatase, rutile and brookite and rutile is the most common as the metastable polymorph. Each polymorph has different band gap positions. Anatase's band gap is 3.2 eV, higher than rutile's which is 3.0 eV. This difference in the band gap will determine their optimum UV wavelength range to promote a photocatalytic process. There are different methods to assess the photocatalytic activity of a material. The most commonly used method is the degradation of a dye in aqueous solution under UV light, due to its simplicity. Under these conditions the decomposition rate of a suitable organic dye is used as a measure of activity. Physical properties such as particle size and surface area will determine the effective area that will interact and absorb the dye prior to degradation. The physical mechanisms involved in such aqueous based methods differ from gas phase reactions. More advanced techniques use mass spectrometers to evaluate photocatalytic activity of titanium dioxide in the gas phase. An effective photocatalyst for heterogeneous reactions in the gas phase is one which is efficient at creating radicals as a result of an absorbed photon.

Keywords: photocatalysis, UV irradiation, nitrogen dioxide, methylene blue reduction, mass spectrometer

1. Introduction

The increase in the worldwide population demands resources and a constant energy supply, leading to an increment of pollutants, as reported by the Intergovernmental Panel on Climate Change released in March 2014 [1]. The report indicated actions must be taken immediately for

the mitigation of climate change. Anthropogenic greenhouse gases such as carbon dioxide, sulphur and nitrous oxides contribute significantly to global warming. Governments and international organizations such as The European Union and the United States of America set maximum levels for emissions of NO_2 and SO_2 amongst others [2].

Since 1972, when Fujishima and Honda discovered the photocatalytic properties of titanium dioxide (TiO_2), the research has been driven by the potential applications of photocatalysis for pollution remediation. Under UV radiation, TiO_2 can create free radicals on its surface by promoting electrons to the conduction band. The available hole which is very reactive and the electron can react with adsorbed water or oxygen to create free radicals and singlet oxygen. The process is illustrated by equations 1–6 [3–6]:

$$TiO_2 \xrightarrow{\quad h\nu \quad} e^- + h^+ \tag{1}$$

$$h^+ + H_2O \rightarrow {}^\bullet OH + H^+ \tag{2}$$

$$e^- + H^+ \rightarrow {}^\bullet H \tag{3}$$

$$H^+ + O_2^{\bullet-} \rightarrow HO_2^\bullet \tag{4}$$

$$e^- + O_2 \rightarrow O_2^{\bullet-} \tag{5}$$

$$h^+ + O_2^{\bullet-} \rightarrow {}^1O_2 \tag{6}$$

One of the most promising applications is the development of novel coatings for both indoor and outdoor urban areas [7–10]. Available commercial photocatalytic coatings cover a range of products, from ceramic tiles with a photocatalytic coating, photocatalytic paints and pigments, antifogging windows to cementitious materials with TiO_2 in its formulation. The application of TiO_2 usually relies on its hydrophilic properties, an excellent advantage for self-cleaning surfaces. To accomplish this, a reliable analytical technique is required to assess the photoactivity of TiO_2 against gaseous pollutants. The photocatalytic activity of various materials is routinely studied for powders whilst in the form of an aqueous suspension. Under these conditions the decomposition rate of a suitable organic dye, such as methylene blue, is used as a measure of activity. This simple method was subsequently standardized in ISO (International Organization for Standardization) 10678. A problem associated with the use of dyes is related to their molecular structure which is not equivalent to typical pollutants. This is the reason that it is difficult to correlate results obtained from methylene blue and an air

pollutant. However, the physical mechanisms involved in such aqueous based methods can be significantly different compared to those of gas-phase reactions, thereby making comparison of relative performance problematic. There are currently a further three published ISO methods related to air purification, each one being specific to a single pollutant:

i.   Nitric oxide (NO) ISO 22197–1

ii.   Acetaldehyde (CH$_3$CHO) ISO 222197–2

iii.   Toluene (CH$_3$C$_6$H$_5$) ISO 22197–3

The aim of this chapter is to assess the photocatalytic activity of commercially available materials by two different techniques (in the aqueous phase as well as the gas phase). Pure TiO$_2$ and photocatalytic coatings specifically developed for use on construction materials were fully characterised and analysed by using X-ray photoelectron spectroscopy (XPS) and X-ray diffraction (XRD), UV-Visible diffusive spectroscopy, Raman spectroscopy, scanning electron microscope (SEM), field emission SEM (FE-SEM) and transmission electron microscopy (TEM).

2. Materials and methods

Four commercially available TiO$_2$ powders were studied. Anatase was supplied by three different companies:

i.   Anatase in the form of Kronos vlp 7000 manufactured by Kronos Titan GmbH [referred to as **7000**]

ii.   Anatase in the form of CristalACTiV™ PC500 manufactured by Crystal Global (85 wt % TiO$_2$, 100% anatase) [referred to as **PC500**]

iii.   Anatase in the form of Aeroxide® P25 manufactured by EVONIK Degussa Industries [referred to as **P25**]

iv.   Rutile in the form of TiPure® R-960 supplied by DuPont (TiO$_2$ > 89 wt %; Al$_2$O$_3$ ~3.3 wt % and amorphous SiO$_2$ ~5.5 wt %) [referred to as **rutile**]

2.1. Characterization of TiO$_2$ powders

Raman Spectroscopy, XPS and XRD were used to characterise the phase composition on the powders. The evaluation of the crystalline phases of the samples were analysed using a Renishaw inVia2012 Raman microscope equipped with diode excitation sources of wavelengths 532 nm and 785 nm.

The XPS equipment used was a Thermo Scientific Theta Probe with a micro-focussed monochromatic Al K$_a$ (1486.6 eV) X-ray source (Thermo Fisher Scientific Inc., Waltham, MA.), with an operating voltage of 12 kV and 3 mA of current. The default spot size was 400 × 800 μm using a flood gun, with a 180° double focussing hemispherical analyser with two-dimension-

al PARXPS detector in an operating vacuum of 10^{-8} mbar. The software CASAXPS 2.3.16 RP 1.6 (Casa Software Ltd., Teingmouth, Devon, UK) was used for data analysis and peak fitting. The adventitious hydrocarbon C 1s peak at 284.8 eV was used to correct for the shift in binding energy attributed to surface charging of the specimen. The XRD equipment used was a Bruker D8 ADVANCE X-ray diffractometer with CuK_α radiation (at 40 kV and 40 mA emission current) equipped with a graphite monochromator and a NaI scintillation detector. 2θ scans were recorded within the range of 20° to 60° with a step of 0.016° and a step time of 269 s.

The bandgap of the photocatalysts was calculated from their reflectance. A PerkinElmer 750 S UV/Vis Spectrometer with a 60 mm Integrating Sphere in a wavelength range between 240 nm and 800 nm was used to measure the reflectance of the TiO_2 powders. The reflectance data was converted into the absorption energy using the Kubelka-Munk equation alongside the Tauc's plot, allowed conversion of the reflectance into absorption energy which corresponds to the band gap [11–13].

The surface morphology and particle size of nanostructured of TiO_2 powders was characterised using FESEM and TEM as together they cover a suitable range of magnifications. A JEOL FESEM6301F equipped with a motorised stage, allowing low accelerating voltages from 1kV to 10kV and TEM (JEOL JEM 1200 EXII with a tungsten filament equipped with a motorised stage, and a Gatan Dual View camera) with working accelerating voltages of 120 kV.

2.2. Evaluation of photocatalytic performance

The photocatalytic activity of the commercial powders was tested by following the degradation of a dye in the aqueous phase and the degradation of NO_2 and CO_2 in the gas phase. Specimens were irradiated under two different UV sources comprising 4×4 arrays of 16 individual GaN UV-LED's. LEDs of wavelength 376–387 nm provided a maximum intensity at 380 nm with a total intensity at the specimen surface of 4.7 W/m².

2.2.1. Photocatalytic degradation of methylene blue

Three tests were undertaken for each TiO_2 powder; one in the dark, to evaluate the amount of dye which was absorbed by the powders; and two tests under UV light. Photocatalytic activity of TiO_2 in solution was studied by following the decrease in the solution's absorption using a Jenway 6300 UV-Visible spectrophotometer. The organic dye methylene blue was used as an indicator.

2.2.2. Photocatalytic degradation of gaseous pollutants

To assess the photocatalytic activity of TiO_2 powders in the gas phase, a mass spectrometer was employed due to its ability to monitor a range of species simultaneously. The system has been reported previously in detail [14–16], including the ionic species and corresponding masses commonly formed in the gas phase [15]. A schematic diagram of the system is shown in **Figure 1**.
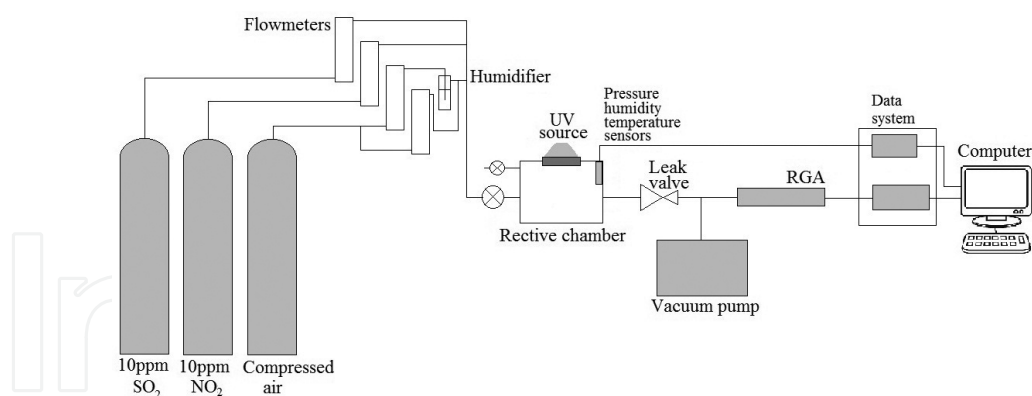
Figure 1. Diagram of the mass analyser. Gas cylinders are connected via flowmeters to the reactive chamber. One output is connected to the detector [15].

TiO$_2$ powders were compressed into 13 mm diameter pellets using a uniaxial press at 500 MPa. The experiments were carried out at 25°C and atmospheric pressure for 150 min inside the chamber. The LED's intensity was 30 W/m². Air was mixed with 203 ppm of NO$_2$ diluted in N$_2$ to provide enough O$_2$ and H$_2$O for TiO$_2$ to initiate photocatalytic reactions, leading an initial concentration of 190 ppm of NO$_2$.

3. Results and discussion

3.1. Electron microscopy

Calculated particle sizes, specific surface area, bandgap and crystallite size are given in **Table 3**.

			7000	PC500	P25	Rutile TiPure
Binding energy (eV) /	**C 1s**	**C-N**	**286.7**/3.7	**286.4**/5.4	**287.1**/5.6	–
Relative concentration (at. %)		**CO$_3$**$^{2-}$	**288.7**/1.8	**289.6**/4.5	–	**288.9**/5.2
	O 1s	**TiO$_2$**	**529.6**/57.1	**529.5**/37	**529.1**/59.9	**529.8**/71.3
		CO$_3$ $^{2-}$	**531.0**/11.5	**531.4**/18.9	**531.3**/7.8	–
		SiO$_2$	–	**533.2**/1.7	–	**533.2**/9.1
	Ca 2p	**Ca**	–	**347.4**/2.6	–	–
	(CaCO$_3$)	**2p$_{3/2}$**				
		Ca 2p$_{1/2}$	–	**350.8**/1.3	–	–
	Si 2p (SiO$_2$)	**Si 2p**	–	**103.2**/2.2	–	**102.8**/12.3
	Ti 2p (TiO$_2$)	**Ti 2p$_{3/2}$**	**458.4**/17.4	**458.5**/17.6	**458.4**/17.9	**458.1**/1.3
	Ti 2p (TiO$_2$)	**Ti 2p$_{1/2}$**	**464.1**/8.5	**464.2**/8.8	**464.1**/8.8	**463.8**/0.7

Table 1. Element ratios and chemical state derived from XPS analysis.

	Lattice plane	7000 (Å)	PC500 (Å)	P25 (Å)	Rutile (Å)
Anatase	(101)	3502	3496	3518	–
	(004)	2375	2384	2377	–
	(112)	–	–	2486	–
	(200)	1896	1889	1891	–
	(105)	1684	1675	1699	–
	(211)	–	–	2,33113	–
	(118)	1485	1483	1480	–
	(116)	–	–	1668	–
Rutile	(110)	–	–	3245	3200
	(101)	–	–	–	2460
	(200)	–	–	–	2276
	(111)	–	–	–	2166
	(210)	–	–	–	2037
	(211)	–	–	1687	1677
	(220)	–	–	–	1614
	(002)	–	–	–	1472
	(310)	–	–	–	1445
	(301)	–	–	–	1354

Table 2. d spacing Calculated from the X-ray diffraction data of rutile and anatase powders.

	Particle size (nm)*	Average particle size (nm)	Crystallite size(nm)	BET (m²/g)*	BET (m²/g)	Band gap (eV)
7000	15	<10	10.1	>250	225	3.37
PC500	5–10	20.8	9.5	350	312	3.35
P25	21	29.8	22.6	35–65	13	3.25
Rutile	500	402	50	-	3.3	3.00

*From producer's datasheet.

Table 3. Particle size, BET and optical band gap for TiO_2 powders.

	Absorbed dye (%) in the dark	Degraded dye (%) under λ=376–387 nm	Degraded dye (%) under λ=381–392 nm
7000	18.2	94.7	39.9
PC500	14.8	98.8	95.23
P25	18.2	99.8	92.8
Rutile	16.3	26.3	16.6

Table 4. Percentage of absorbed and degraded dye after 60 min under two different UV LED and in the dark.

3.1.1. 7000

Anatase 7000 presented a distribution of micro and nanoparticles as shown in **Figure 2**. TEM revealed an agglomeration of nanoparticles (>10 nm), being unable to determine an average particle size.
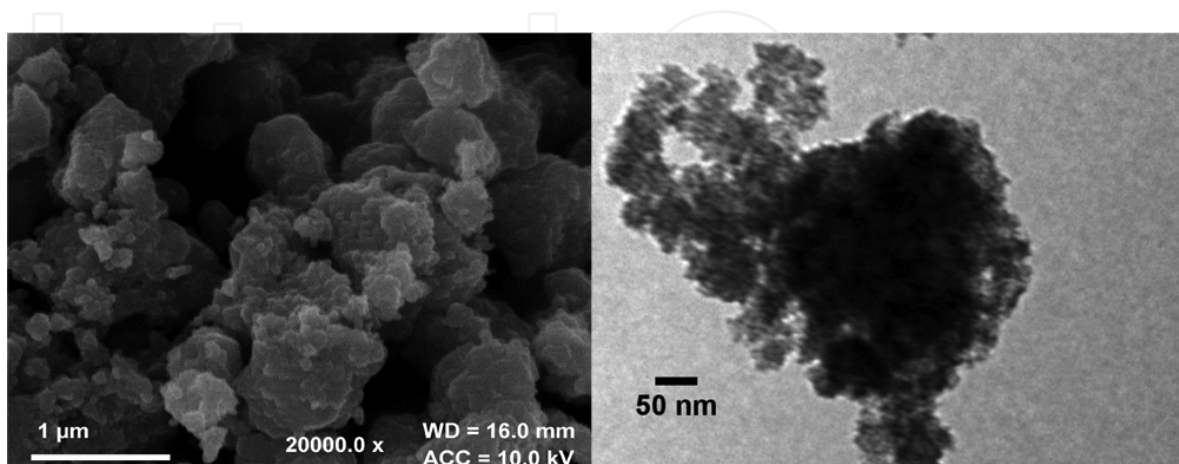

Figure 2. FESEM (left) and TEM (right) images of anatase 7000.

3.1.2. PC500

FESEM revealed a large number of particles of ~ 600 nm, whereas TEM showed particles in the range of 20 nm (**Figure 3**).
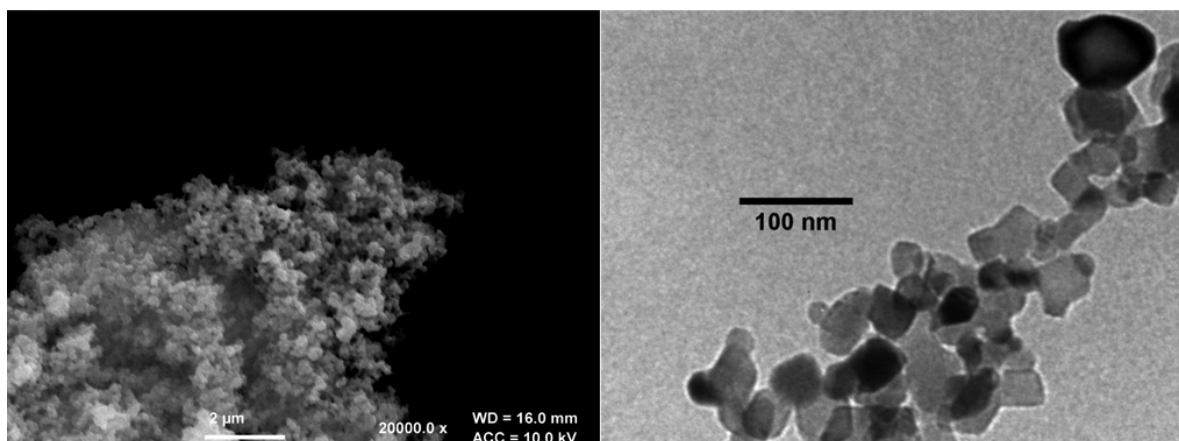

Figure 3. FESEM (left) and TEM (right) images of anatase PC500.

3.1.3. P25

Anatase P25 showed the most homogeneous particle size distribution in FESEM as well as in TEM, held in the range of 30 nm (**Figure 4**).
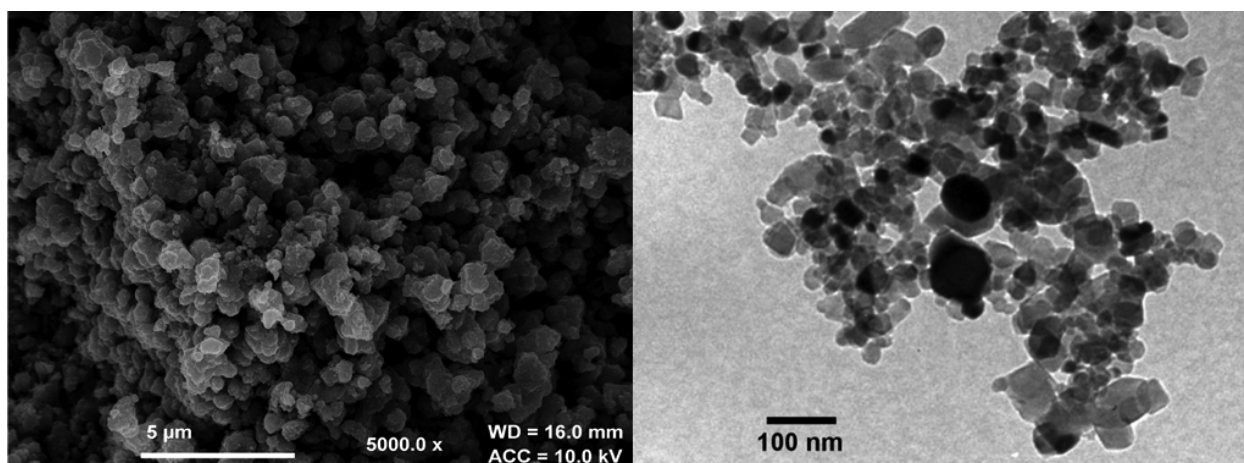
Figure 4. FESEM (left) and TEM (right) images of anatase P25.

3.1.4. Rutile

Rutile TiPure shows a narrow particle size distribution with 400 μm of average particle size. This average particle size was corroborated with sizes estimated from TEM images, as **Figure 5** shows.
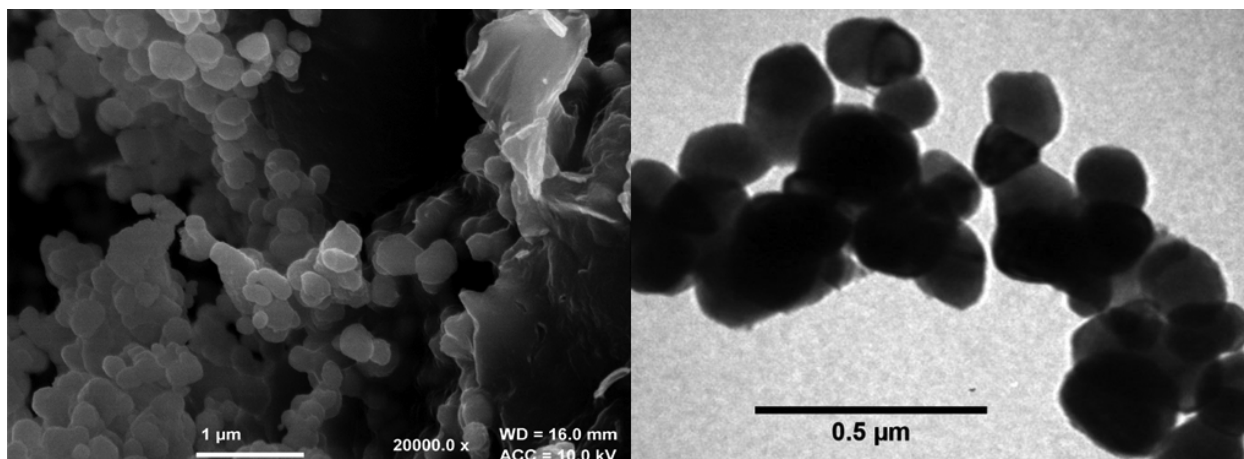
Figure 5. FESEM (left) and TEM (right) images of rutile TiPure.

3.2. Raman spectroscopy

Raman spectroscopy was conducted on the samples before exposure to reactive gases over the range 0–1000 cm^{-1} where the main vibrational modes can be observed. **Figure 6** shows complied Raman spectra form the four TiO$_2$ powders.
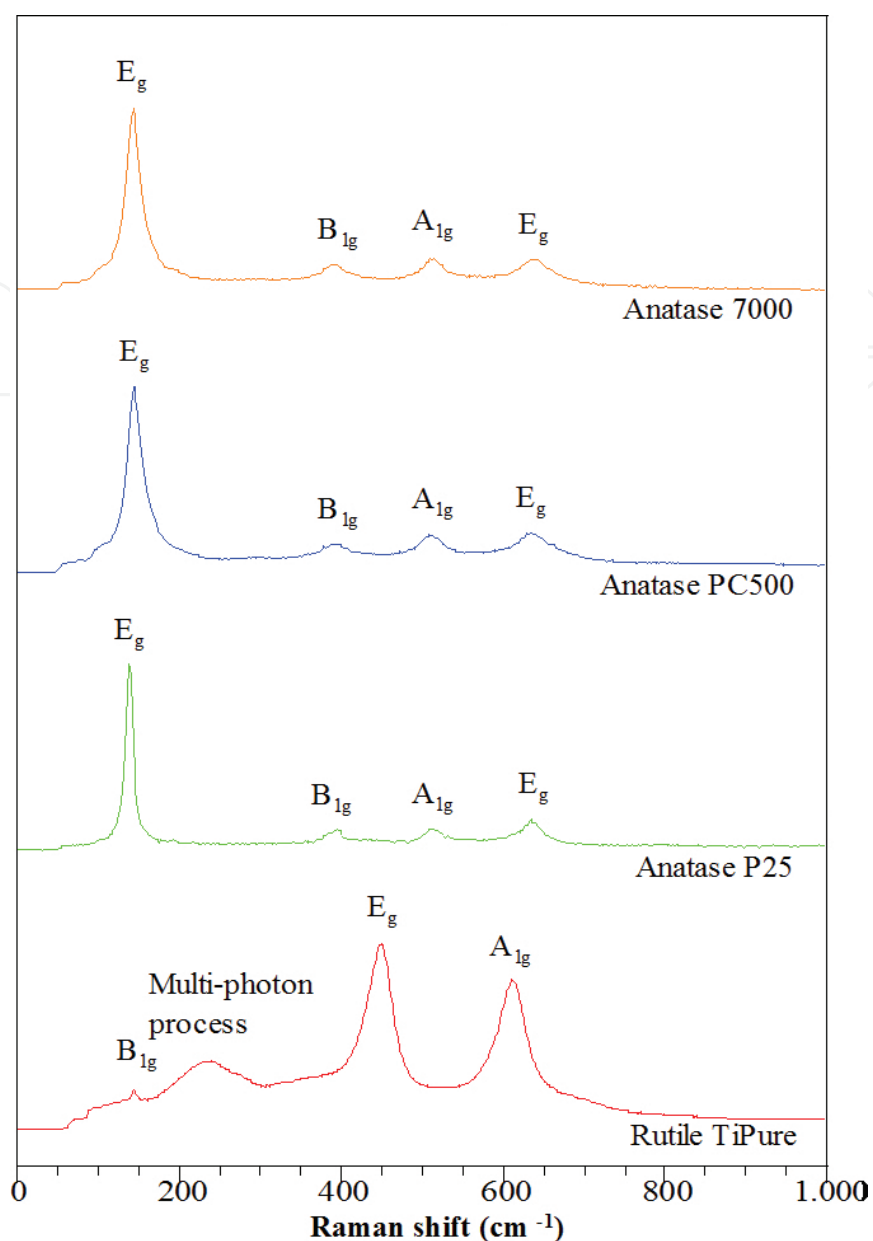
Figure 6. Raman spectra from 0 to 1000 cm^{-1} of four different TiO$_2$ powders.

There are four lattice displacements for rutile which are active in Raman, B$_{1g}$ (145 cm^{-1}) and E$_g$ (445 cm^{-1}, most intense), where O^{2-} anions move relative to the stationary Ti^{4+}; A$_{1g}$ (610 cm^{-1}) which is an asymmetric bending vibration of O-Ti-O, and a multi-phonon process (240 cm^{-1}) [17–20].

For anatase, there are six lattice displacements which are active in Raman, A$_{1g}$ (513 cm^{-1}), B$_{1g}$ (399 and 519 cm^{-1}) and E$_g$ (144, 197 and 639 cm^{-1}) caused by Ti-O bond stretching and bending of the O-Ti-O bond [21, 22]. The peak at 197 cm^{-1} assigned to the E$_g$ mode is very weak and is not listed in **Figure 6** due to its low intensity (0.05%). The peak B$_{1g}$ at 519 cm^{-1} was reported at 73 K and it is not visible at room temperature.

3.3. X-ray photoelectron spectroscopy

Figure 7 shows a typical survey spectra of TiO_2 (P25) and **Table 1** shows the binding energies and elemental ratios for carbon, oxygen, calcium, silicon and titanium, calculated from higher resolution spectra in specific regions for the commercial powders.
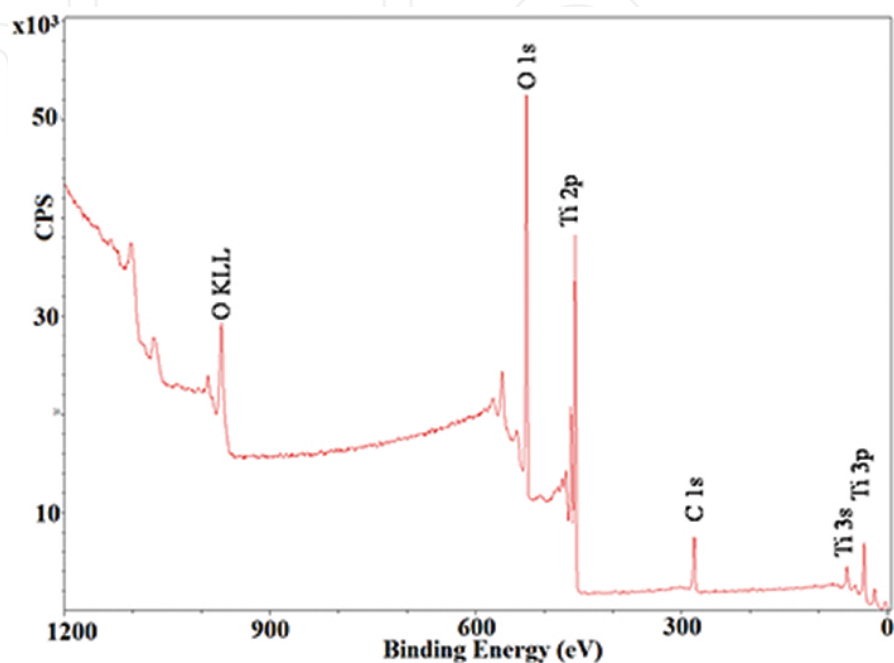

Figure 7. XPS spectra of anatase P25.

As **Table 1** shows, KRONOS vlp 7000 and Aeroxide® P25 are the purest TiO_2 powders, whereas PC500 and Rutile TiPure® contain $CaCO_3$ and SiO_2 impurities.

Binding energies for TiO_2 related to Ti 2p peaks varied between 458.1 and 458.5 eV in accordance with previous studies [23, 24], and for O 1s the observed peaks are within the range of 528.8–529.8 eV. These results agreed with studies carried by Dementjev [23] and Erdem [24], where the Ti 2p binding energies ranged from 458.0 to 459.4 eV and for O 1s ranged from 529.4 to 530.6 eV.

Peaks corresponding to C 1s were assigned to adventitious carbon with a binding energy of 284.8 eV and were used to calibrate the spectrum for charging and a second peak corresponding to CO_3^{2-} in 7000, PC500 and rutile TiO_2 powders. The binding energy of this peak in the different powders ranged between 288.7 and 289.6 eV which is in agreement with studies by Kang et al. [25] and Demri and Muster [26] who report $CaCO_3$ binding energies of 288.6 and 289.2eV. The binding energy for the Ca 2p peak identified at 347.4 eV was in agreement with previous studies by Stipp [27] who reported a $CaCO_3$ binding energy of 347.7 eV. For SiO_2, the reported values for the O 1s peak at 533.2 eV and ~103 eV is also in agreement with previous studies [28].

3.4. X-ray diffraction

XRD was undertaken to characterise the crystal phase of the powders. **Figure 8** compares the normalised diffractograms for anatase (PC500, 7000 and P25) and rutile crystals. Previous studies were used to identify and label peaks from different crystal phases [20, 21, 29–32] and **Table 2** compares the lattice d spacing for those peaks.
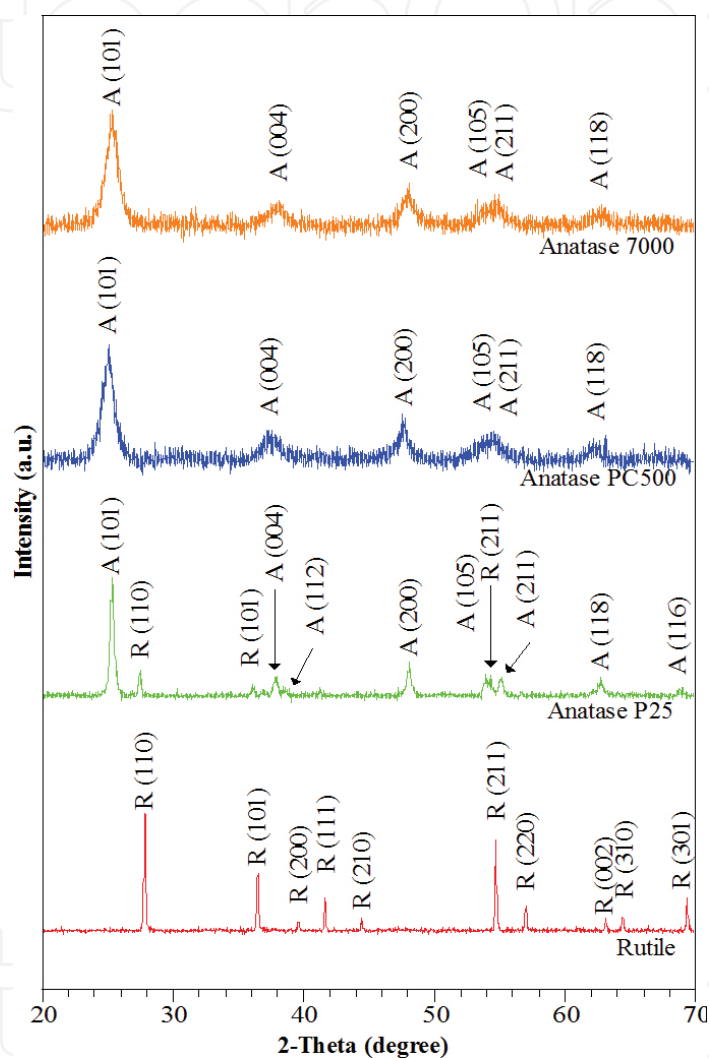

Figure 8. X-ray diffractogram of rutile and anatase powders.

In the case of anatase, the P25 diffractogram is sharper than the PC500 and 7000, revealing more peaks that correspond to anatase. It also shows 12% rutile (by comparing the maximum intensity of anatase crystallographic plane (101) with the maximum of rutile's (110)). For PC500 and 7000, fewer peaks are observed compared to the P25. This is attributed to internal strains within the crystals and lattice defects broadening the peaks causing subsequent overlap.

From Scherrer's equation, the crystallite size was calculated from the most intense peaks for each powder. The values are presented in **Table 3** which compiles other results.

3.5. UV–vis diffusive spectroscopy

UV-Visible reflectance of powders was measured from 250 to 800 nm for all the commercial powders. **Figure 9** shows the reflectance of TiO_2 particles over a wavelength range on the abscissa. The plot shows that, PC500 has a drop in the reflectance at 405 nm, 7000 at 377 nm, P25 at 381 and rutile at 371 nm.
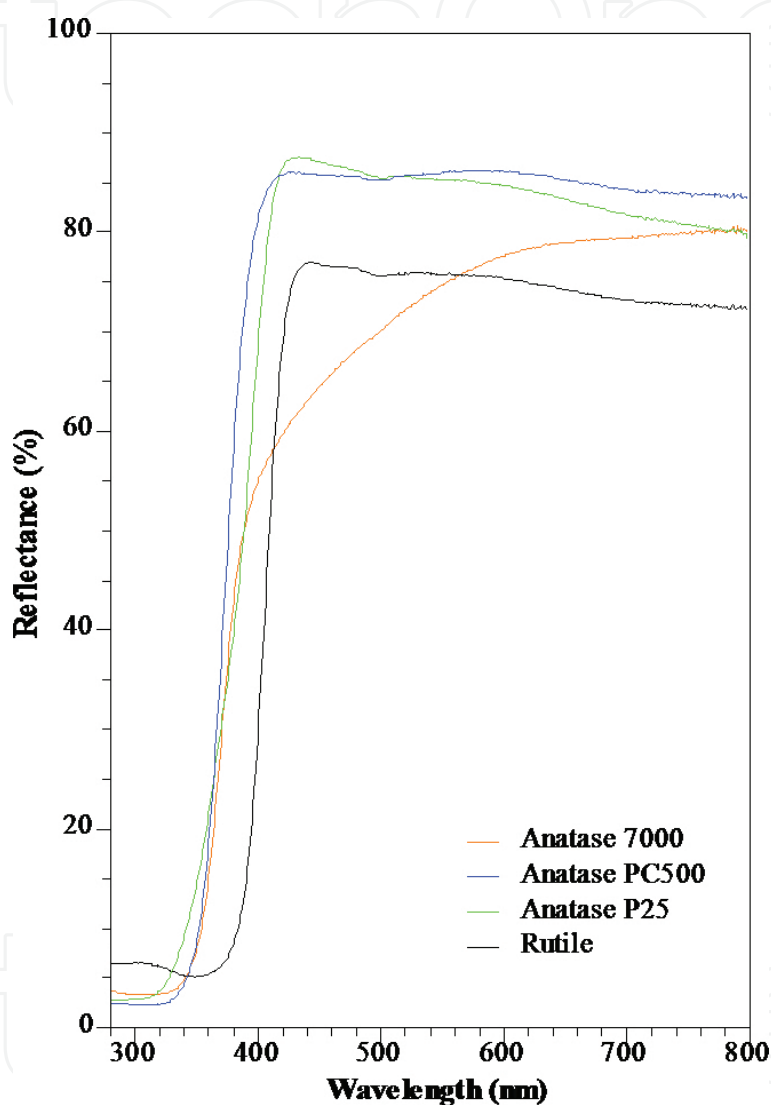

Figure 9. Graphical representation of reflectance against wavelength for rutile and anatase powders.

Table 3 compiles the calculated optical band gap, BET surface area, average crystallite size (from XRD diffractogram using Scherrer's equation) and average particle size calculated from TEM images. It also contains particle size and BET from the material safety data sheets.

Particle size and BET results agreed with the information in the technical data sheets of anatase nanoparticles, and also with reported values in the literature [13, 33, 34]. As the 7000 consisted of aggregates of nanoparticles, it was not possible to report an average particle size, as

shown in **Figure 2**. From the TEM images the size of the individual nanoparticles forming the agglomerates was less than 10 nm. Scherrer equation's estimations are close to the calculated values from TEM and FE-SEM. For the case of rutile, the estimated crystallite size was 50 nm. A possible explanation for the difference of an order of magnitude is that particles are formed from different grains; where the crystallite size is the size of those grains.

The estimated band gaps for anatase powders range from 3.37 eV (for 7000) to 3.25 eV (for P25). Although these results show a small discrepancy in the band gap determination, previous researchers reported different values for P25 (3.10–3.15 eV) [13, 34]; as well as for 7000, carbon doped, which has band gap higher than 3.2 eV [35, 36]. PC500 also exhibits a wider band gap than reported previously. For the PC500 and 7000 band gaps, the optimum wavelength was 370 nm. Rutile's band gaps agree with the reported values for M. Kete, D. Reyes-Coronado and K. Madhusudan Reddy [33, 37, 38].

3.6. Photocatalytic performance

3.6.1. Photocatalytic degradation of methylene blue

Figure 10 shows the degradation of methylene blue for sixty minutes, and **Table 4** collates the dye removed per specimen under irradiation at different wavelengths.
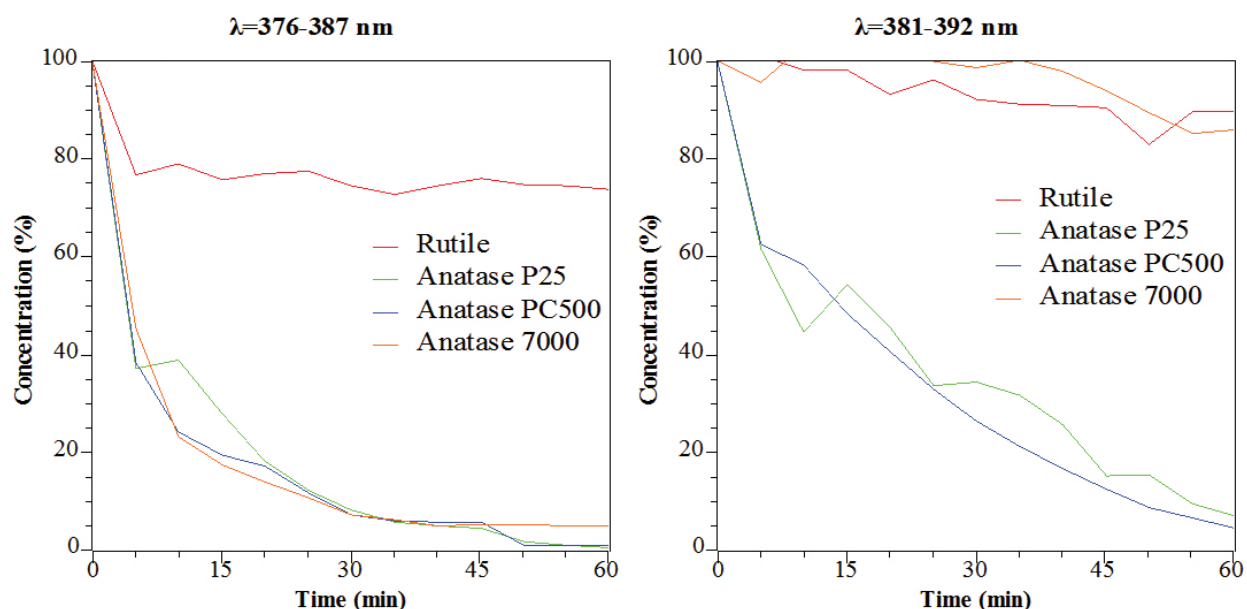

Figure 10. Photo-oxidation of an aqueous solution of methylene blue under different UV LED (I=4.7 W/m^2) for TiO$_2$ powders.

Anatase P25 and PC500 successfully degraded more than 90% of methylene blue under different UV light. In the case of 7000, the difference in its photoreactivity under different wavelengths is remarkable. Whereas P25 band gaps are in the 387 nm wavelength region, PC500 and 700 band gaps are in the 370 nm region. This is the reason why under a wavelength range 381–392 nm, 7000 was not able to degrade more than 40% of dye; whereas

under 376–387 nm, 95% of methylene blue was degraded. Under the irradiation of the UV LED of 376–387 nm, 7000 received more photons with the required energy to initiate the photocatalytic process.

For rutile, if the percentage of absorbed dye is considered, it only worked as a photocatalyst under the UV LED with a wavelength of 381–392 nm, near to its band gap (413 nm) degrading less than 26%.

3.6.2. Photocatalytic degradation of gaseous pollutants

Figures 11–14 show the fractional change of CO_2, NO_2, H_2O and O_2 related to Ar.
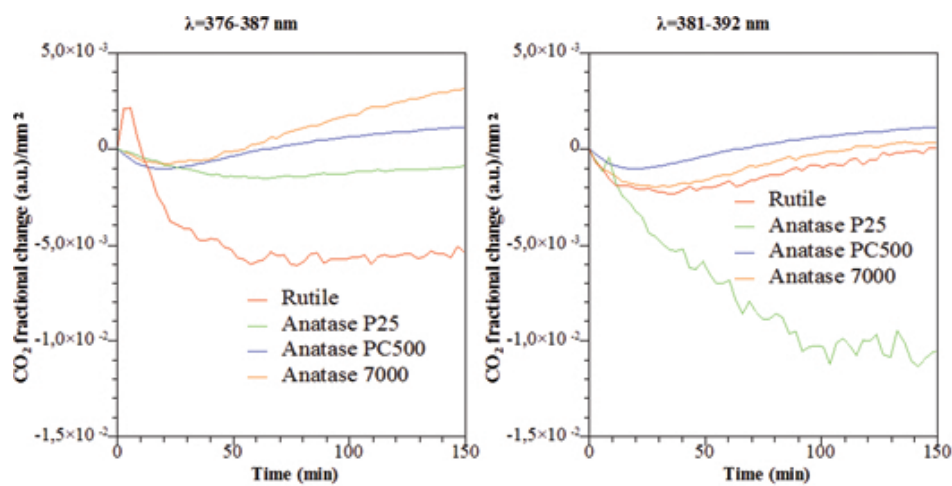

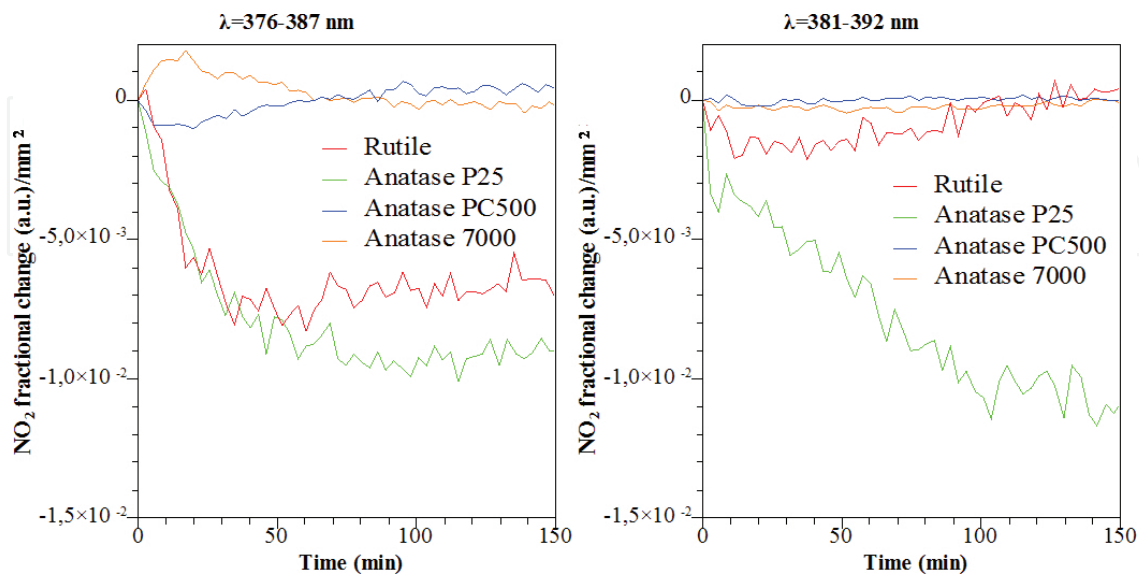**Figure 11.** Fractional reduction of CO_2 related to Ar over time under different conditions.

Figure 12. Fractional reduction of NO_2 related to Ar over time under different conditions.

Figure 13. Fractional reduction of H_2O related to Ar over time under different conditions.

Figure 14. Fractional reduction of O_2 related to Ar over time under different conditions.

Figure 15. Proposed mechanism of photo-oxidation of CO_2.

The high photoreactivity TiO_2 powders show degradation of methylene blue in the aqueous phase, however their reactivity in the gas phase was different. Not all the commercial anatase powders were able to degrade NO_2 and CO_2, only P25 removed those molecules successfully. Rutile, which was not effective in aqueous solution, was able to remove CO_2 and NO_2 under UV irradiation. Rutile's band gap is 370 nm, which made it more photoactive under the UV LED of wavelength of 376–387 nm, as its band gap is held.

When evaluating the photocatalytic TiO_2 powders, it is noteworthy that their sizes and physical properties differ from each other. Anatase 7000 has the smallest particle size and highest specific surface area whereas rutile exhibits the largest particle size and smallest specific surface area.

The phase (liquid or gas) in which the particles are evaluated has important influences upon the performance observed. In the gas phase, probabilities of direct contact of TiO_2 surface with the molecules of interest (H_2O and O_2 to create radicals) and thereafter the collision of those radicals with NO_2 and CO_2 is much smaller than in the aqueous phase.

For anatase PC500 and 7000, the high efficiency in the photodegradation of methylene blue is due to the low particle size and high specific surface area, which increase the contact of the exposed surface to H_2O and UV light. When analysed in gas phase, they showed a lower photon/e^--h^+ conversion yield, and were unable to promote a photocatalytic reaction under UV exposure at both the wavelength ranges tested.

Figures 13 and 14 show the fractional change of H_2O and O_2 with time, which are required in the photocatalytic process to generate radicals. The figures illustrate that the decay of O_2 corresponds to the decomposition of CO_2 and H_2O, as with NO_2.

The reaction of NO_2 and H_2O promoted by TiO_2 under UV light has been previously reported, forming HNO_3 as the reaction product [39–42]. Under wavelength 376–387 nm in the gas phase removal of NO_2 was observed alongside that of H_2O. Whereas when irradiating under 381–392 nm, not only were NO_2 and H_2O were removed from the atmosphere, but also O_2 and CO_2 were consumed in the same ratio.

This can be explained by anatase's bandgap reported value 3.2 eV [38, 42], which is held in the range of the UV LED of wavelength 381–392 nm, as **Figure 11** shows. This difference in energy would be sufficient to promote the radicalisation of O_2 and, subsequently the reaction with CO_2.

The proposed mechanisms for CO_2 removal suggest that the molecule anchors to the photocatalyst's surface, reducing CO_2 into CO and finally into C, desorbing CO and O [43, 44]. This mechanism would not explain the consumption of O_2. Nonetheless, if CO_2 anchors as shown in **Figure 15** the oxidation of CO_2 in the presence of TiO_2 surface absorbed $O_2^{\bullet-}$ could be feasible.

4. Conclusions

The following conclusions can be drawn from the analysis of commercial TiO_2 powders:

- Photocatalytic degradation of methylene blue in aqueous solution is influenced by factors such as particle size and surface area which can influence the measured activity relative to the gas phase reaction.

- Mass spectrometry has been demonstrated as a powerful technique for the assessment of photocatalytic properties in the gas phase.

- From the three commercial available anatase powders, Aeroxide P25 proved to be the most efficient photocatalyst, in the aqueous phase as well as gas phase. Rutile, the most stable polymorph also showed photocatalytic activity.

- The removal of NO_2 in the presence of H_2O, with HNO_3 as the product was observed. The capability of TiO_2 to decompose CO_2 in the presence of O_2 was also noted and a new mechanism proposed.

Acknowledgements

Author details

Manuel Nuño[1*], Richard J. Ball[1] and Chris R. Bowen[2]

*Address all correspondence to: manuelnunotutor@hotmail.com

1 BRE Centre for Innovative Construction Materials, Department of Architecture and Civil Engineering, University of Bath, BA2 7AY, Bath, England

2 Department of Mechanical Engineering, University of Bath, BA2 7AY, Bath, England

References

[1] Contribution of Working Groups I, II and III to the Fifth Assessment Report of the Intergovernmental Panel on Climate Change [Core Writing Team, R.K. Pachauri and L.A. Meyer (eds.)], "IPCC 2014: Climate Change 2014: Synthesis report," Geneva, Switzerland, 2014.

[2] "Directive 2008/50/EC of the European Parliament and of the Council of 21 May 2008 on ambient air quality and cleaner air for Europe."

[3] M. R. Hoffmann, S. T. Martin, W. Choi, and D. W. Bahnemann, "Environmental applications of semiconductor photocatalysis," Chem. Rev., vol. 95, no. 1, pp. 69–96, 1995.

[4] A. Heller, "Chemistry and applications of photocatalytic oxidation of thin organic films," Acc. Chem. Res., vol. 28, no. 12, pp. 503–508, 1995.

[5] D. A. Tryk, A. Fujishima, and K. Honda, "Recent topics in photoelectrochemistry: achievements and future prospects," Electrochim. Acta, vol. 45, no. 15–16, pp. 2363–2376, 2000.

[6] M. Serratos and A. Bronson, "The effect of oxygen partial pressure on the stability of Magneli phases in high temperature corrosive wear," Wear, vol. 198, no. 1–2, pp. 267–270, 1996.

[7] B. Tryba, P. Homa, R. J. Wróbel, and A. W. Morawski, "Photocatalytic decomposition of benzo-[a]-pyrene on the surface of acrylic, latex and mineral paints. Influence of paint composition," J. Photochem. Photobiol. A Chem., vol. 286, pp. 10–15, 2014.

[8] T. Maggos, J. G. Bartzis, M. Liakou, and C. Gobin, "Photocatalytic degradation of NO_x gases using TiO_2-containing paint: A real scale study," J. Hazard. Mater., vol. 146, no. 3, pp. 668–673, 2007.

[9] L. Hochmannova and J. Vytrasova, "Photocatalytic and antimicrobial effects of interior paints," Prog. Org. Coatings, vol. 67, no. 1, pp. 1–5, 2010.

[10] M. Baudys, J. Krýsa, M. Zlámal, and A. Mills, "Weathering tests of photocatalytic facade paints containing ZnO and TiO_2," Chem. Eng. J., vol. 261, pp. 83–87, Feb. 2015.

[11] P. Kubelka, "New contributions to the optics of intensely light-scattering materials part I," J. Opt. Soc. Am., vol. 38, no. 5, p. 448, 1948.

[12] A. Murphy, "Band-gap determination from diffuse reflectance measurements of semiconductor films, and application to photoelectrochemical water-splitting," Sol. Energy Mater. Sol. Cells, vol. 91, no. 14, pp. 1326–1337, 2007.

[13] R. López and R. Gómez, "Band-gap energy estimation from diffuse reflectance measurements on sol–gel and commercial TiO_2: a comparative study," J. Sol–gel Sci. Technol., vol. 61, no. 1, pp. 1–7, 2012.

[14] M. Nuño, R. J. Ball, C. R. Bowen, R. Kurchania, and G. D. Sharma, "Photocatalytic activity of electrophoretically deposited (EPD) TiO_2 coatings," J. Mater. Sci., vol. 50, no. 14, pp. 4822–4835, 2015.

[15] M. Nuño, R. J. Ball, and C. R. Bowen, "Study of solid/gas phase photocatalytic reactions by electron ionization mass spectrometry," J. Mass Spectrom., vol. 49, no. 8, pp. 716–726, 2014.

[16] M. Nuño, G. L. Pesce, C. R. Bowen, P. Xenophontos, and R. J. Ball, "Environmental performance of nano-structured Ca(OH)₂/TiO₂ photocatalytic coatings for buildings," Build. Environ., vol. in press, 92, pp. 734–742, 2015.

[17] Y. Zhang, C. X. Harris, P. Wallenmeyer, J. Murowchick, and X. Chen, "Asymmetric Lattice Vibrational Characteristics of Rutile TiO₂ as Revealed by Laser Power Dependent Raman Spectroscopy," J. Phys. Chem. C, vol. 117, no. 45, pp. 24015–24022, 2013.

[18] T. Lan, X. Tang, and B. Fultz, "Phonon anharmonicity of rutile TiO₂ studied by Raman spectrometry and molecular dynamics simulations," Phys. Rev. B, vol. 85, no. 9, p. 094305, 2012.

[19] G. A. Samara and P. S. Peercy, "Pressure and Temperature Dependence of the Static Dielectric Constants and Raman Spectra of TiO₂ (Rutile)," Phys. Rev. B, vol. 7, no. 3, pp. 1131–1148, 1973.

[20] M. Rezaee, S. M. Mousavi Khoie, and K. H. Liu, "The role of brookite in mechanical activation of anatase-to-rutile transformation of nanocrystalline TiO₂: An XRD and Raman spectroscopy investigation," CrystEngComm, vol. 13, no. 16, p. 5055, 2011.

[21] W. F. Zhang, Y. L. He, M. S. Zhang, Z. Yin, and Q. Chen, "Raman scattering study on anatase TiO₂ nanocrystals," J. Phys. D. Appl. Phys., vol. 33, no. 8, p. 912, 2000.

[22] T. Ohsaka, F. Izumi, and Y. Fujiki, "Raman spectrum of anatase, TiO₂," J. Raman Spectrosc., vol. 7, no. 6, pp. 321–324, 1978.

[23] A. P. Dementjev, "Altered layer as sensitive initial chemical state indicator∗," J. Vac. Sci. Technol. A Vacuum, Surfaces, Film., vol. 12, no. 2, p. 423, 1994.

[24] B. Erdem, R. A. Hunsicker, G. W. Simmons, E. D. Sudol, V. L. Dimonie, and M. S. El-Aasser, "XPS and FTIR Surface Characterization of TiO₂ Particles Used in Polymer Encapsulation," Langmuir, vol. 17, no. 9, pp. 2664–2669, 2001.

[25] I.-C. Kang, Q. Zhang, S. Yin, T. Sato, and F. Saito, "Preparation of a visible sensitive carbon doped TiO₂ photo-catalyst by grinding TiO₂ with ethanol and heating treatment," Appl. Catal. B Environ., vol. 80, no. 1–2, pp. 81–87, 2008.

[26] B. Demri and D. Muster, "XPS study of some calcium compounds," J. Mater. Process. Technol., vol. 55, no. 3–4, pp. 311–314, 1995.

[27] S. L. Stipp and M. F. Hochella, "Structure and bonding environments at the calcite surface as observed with X-ray photoelectron spectroscopy (XPS) and low energy electron diffraction (LEED)," Geochim. Cosmochim. Acta, vol. 55, no. 6, pp. 1723–1736, 1991.

[28] T. Gross, M. Ramm, H. Sonntag, W. Unger, H. M. Weijers, and E. H. Adem, "An XPS analysis of different SiO₂ modifications employing a C 1s as well as an Au 4f7/2 static charge reference," Surf. Interface Anal., vol. 18, no. 1, pp. 59–64, 1992.

[29] R. J. T. and P. K. S. and R. G. K. and R. V Jasra, "Photocatalytic degradation of dyes and organic contaminants in water using nanocrystalline anatase and rutile TiO_2," Sci. Technol. Adv. Mater., vol. 8, no. 6, p. 455, 2007.

[30] Y. F. You, C. H. Xu, S. S. Xu, S. Cao, J. P. Wang, Y. B. Huang, and S. Q. Shi, "Structural characterization and optical property of TiO_2 powders prepared by the sol–gel method," Ceram. Int., vol. 40, no. 6, pp. 8659–8666, 2014.

[31] B. K. Mutuma, G. N. Shao, W. D. Kim, and H. T. Kim, "Sol–gel synthesis of mesoporous anatase-brookite and anatase-brookite-rutile TiO_2 nanoparticles and their photocatalytic properties.," J. Colloid Interface Sci., vol. 442, pp. 1–7, 2015.

[32] D. M. Tobaldi, M. P. Seabra, G. Otero-Irurueta, Y. R. de Miguel, R. J. Ball, M. K. Singh, R. C. Pullar, and J. A. Labrincha, "Quantitative XRD characterisation and gas-phase photocatalytic activity testing for visible-light (indoor applications) of KRONOClean 7000[registered sign]," RSC Adv., vol. 5, no. 124, pp. 102911–102918, 2015.

[33] M. Kete, E. Pavlica, F. Fresno, G. Bratina, and U. Štangar, "Highly active photocatalytic coatings prepared by a low-temperature method," Environ. Sci. Pollut. Res., vol. 21, no. 19, pp. 11238–11249, 2014.

[34] K. Nagaveni, M. S. Hegde, N. Ravishankar, G. N. Subbanna, and G. Madras, "Synthesis and structure of nanocrystalline TiO_2 with lower band gap showing high photocatalytic activity," Langmuir, vol. 20, no. 7, pp. 2900–2907, 2004.

[35] T. M. Triantis, T. Fotiou, T. Kaloudis, A. G. Kontos, P. Falaras, D. D. Dionysiou, M. Pelaez, and A. Hiskia, "Photocatalytic degradation and mineralization of microcystin-LR under UV-A, solar and visible light using nanostructured nitrogen doped TiO_2," J. Hazard. Mater., vol. 211–212, pp. 196–202, 2012.

[36] A. Manassero, M. L. Satuf, and O. M. Alfano, "Evaluation of UV and visible light activity of TiO_2 catalysts for water remediation," Chem. Eng. J., vol. 225, pp. 378–386, 2013.

[37] D. Reyes-Coronado, G. Rodríguez-Gattorno, M. E. Espinosa-Pesqueira, C. Cab, R. de Coss, and G. Oskam, "Phase-pure TiO_2 nanoparticles: anatase, brookite and rutile," Nanotechnology, vol. 19, no. 14, p. 145605, 2008.

[38] K. Madhusudan Reddy, S. V Manorama, and A. Ramachandra Reddy, "Bandgap studies on anatase titanium dioxide nanoparticles," Mater. Chem. Phys., vol. 78, no. 1, pp. 239–245, 2003.

[39] S. Daito, T. Watanabe, and F. Tochikubo, "NO x Removal Process in Pulsed Corona Discharge Combined with TiO_2 Photocatalyst," Jpn. J. Appl. Phys., vol. 40, no. 4R, p. 2475, 2001.

[40] N. Negishi, K. Takeuchi, and T. Ibusuki, "Surface structure of the TiO_2 thin film photocatalyst," J. Mater. Sci., vol. 33, no. 24, pp. 5789–5794, 1998.

[41] Y. Bedjanian and A. El Zein, "Interaction of NO$_2$ with TiO$_2$ surface under UV irradiation: products study," J. Phys. Chem. A, vol. 116, no. 7, pp. 1758–1764, 2012.

[42] Y.-M. Lin, Y.-H. Tseng, J.-H. Huang, C. C. Chao, C.-C. Chen, and I. Wang, "Photocatalytic activity for degradation of nitrogen oxides over visible light responsive titania-based photocatalysts," Environ. Sci. Technol., vol. 40, no. 5, pp. 1616–1621, 2006.

[43] M. Anpo, H. Yamashita, Y. Ichihashi, and S. Ehara, "Photocatalytic reduction of CO$_2$ with H$_2$O on various titanium oxide catalysts," J. Electroanal. Chem., vol. 396, no. 1–2, pp. 21–26, 1995.

[44] M. Anpo, H. Yamashita, K. Ikeue, Y. Fujii, S. G. Zhang, Y. Ichihashi, D. R. Park, Y. Suzuki, K. Koyano, and T. Tatsumi, "Photocatalytic reduction of CO$_2$ with H$_2$O on Ti-MCM-41 and Ti-MCM-48 mesoporous zeolite catalysts," Catal. Today, vol. 44, no. 1–4, pp. 327–332, 1998.